Enhanced High-Temperature Electronic Transport Properties in Nanostructured Epitaxial Thin Films of the $La_{n+1}Ni_nO_{3n+1}$ Ruddlesden−Popper Series ($n = 1, 2, 3, \infty$)

Mónica Burriel,[†] Gemma Garcia,[‡] Marta D. Rossell,[§] Albert Figueras,[†] Gustaaf Van Tendeloo,[§] and José Santiso*[,†,||]

ICMAB/CSIC, Campus UAB, 08193 Bellaterra, Spain, Grup de Nanomaterials i Microsistemes, Departament de Física, UAB, 08193 Bellaterra Spain, and EMAT, University of Antwerp, Groenenborgerlaan 171, B-2020, Antwerp, Belgium

Received March 23, 2007. Revised Manuscript Received May 30, 2007

Epitaxial thin films of lanthanum nickel oxide Ruddlesden−Popper series ($La_{n+1}Ni_nO_{3n+1}$) have been prepared on different single-crystal substrates by metal organic chemical vapor deposition. Varying the La/Ni composition ratio in the precursor solution allows deposition of films with controlled La/Ni stoichiometry ranging between 1 and 2. Epitaxial La_2NiO_4 ($n = 1$) and $LaNiO_3$ ($n = \infty$) pure phases were obtained for La/Ni close to 2 and 1, respectively. For intermediate La/Ni composition, films with a microstructure consisting of a disordered stacking of nanodomains with progressively increasing average n value were obtained. Similarly with bulk samples, the electronic conductivity of the nanostructured films increases with the measured average n value, opening the possibility to prepare new mixed ionic and electronic conducting nanocomposite thin films with tailored properties

1. Introduction

The research on new oxide materials with both high ionic and electronic conductivity (MIEC: mixed ionic and electronic conductors) is of key importance in order to achieve optimum performance in different electrochemical devices such as solid oxide fuel cells (SOFCs), gas sensors, oxygen membrane generators, catalytic oxidation systems, etc.[1−5] Particularly, in these applications there is a major interest in reducing the working temperatures to about 500−600 °C. Under such reduced temperature conditions, the surface activity of the materials becomes one of the major limiting steps for the device performance. Therefore, the control over the electronic conductivity of the MIEC material, which is directly related to the oxygen surface exchange kinetics, becomes a crucial issue. Among the different types of MIEC oxides there has been a large interest in perovskite-related materials such as $La_2NiO_{4+\delta}$, and doped materials based on this compound, because of its high ionic and electronic mobilities.[6−12] It presents a K_2NiF_4-type layered structure, which alternates $LaNiO_3$ perovskite blocks layers and LaO rock salt layers along the c-axis.[13] It corresponds to the $n = 1$ member of a more general Ruddlesden−Popper (RP) series $La_{n+1}Ni_nO_{3n+1}$,[14−16] where n corresponds to the number of perovskite blocks in the sequence. Different studies on the $n = 1$, 2, 3, or ∞ phases in the literature, reveal that the electronic transport in $La_{n+1}Ni_nO_{3n+1}$ depends to a large extent on the number of perovskite blocks, gradually varying from an insulating to a metallic behavior upon increasing n.[17−21] These changes are mainly associated with variations in the Ni valence state from Ni^{2+} for $n = 1$ member (La_2NiO_4) to Ni^{3+} for the $n = \infty$ member ($LaNiO_3$), along with the oxygen content.[14] Very recently there has been a renewed interest to study the electrical properties of these compounds in view of their potential application as cathodes for SOFCs.[22]

* Corresponding author. E-mail: santiso@icmab.es.
[†] ICMAB/CSIC.
[‡] UAB.
[§] University of Antwerp.
[||] Present address: Research Center for Nanoscience and Nanotechnology, CIN2. Campus UAB Bellaterra, 08193 Barcelona. Spain. Ph.: +34 935814700.

(1) Steele, B. C. H. *Solid State Ionics* **1996**, *86*−*88*, 1223−1234.
(2) Huijsmans, J. P. P. *Curr. Opin. Solid State Mater. Sci.* **2001**, *5*, 317−323.
(3) Badwal, S. P. S.; Ciacchi, F. T. *Adv. Mater.* **2001**, *13*, 993−996.
(4) Skinner, S. J.; Kilner, J. A. *Mater. Today* **2003**, *6*, 30−37.
(5) Haile, S. M. *Acta Mater.* **2003**, *51*, 5981−6000.
(6) Skinner, S. J.; Kilner, J. A. *Solid State Ionics* **2000**, *135*, 709−712.
(7) Kharton, V. V.; Viskup, A. P.; Naumovich, E. N.; Marques, F. M. B. *J. Mater. Chem.* **1999**, *9*, 2623−2629.
(8) Mauvy, F.; Bassat, J. M.; Boehm, E.; Dordor, P.; Loup, J. P. *Solid State Ionics* **2003**, *158*, 395− 407.
(9) Boehm, E.; Bassat, J. -M.; Steil, M. C.; Dordor, P.; Mauvy F.; Grenier, J.-C. *Solid State Sci.* **2003**, *5*, 973−981.
(10) Bassat, J. M.; Odier, P.; Villesuzanne, A.; Marin, C.; Pouchard, M. *Solid State Ionics* **2004**, *167*, 341−347.
(11) Kharton, V. V.; Yaremchenko, A. A.; Shaula, A. L.; Patrakeev, M. V.; Naumovich, E. N.; Logvinovich, D. I.; Frade, J. R.; Marques, F. M. B. *J. Solid State Chem.* **2004**, *177*, 26−37.
(12) Smith, J. B.; Norby, T. *J. Electrochem. Soc.* **2006**, *153*, A233−A238.
(13) Mehta, A.; Heaney, P. J. *Phys. Rev. B* **1994**, *49*, 563−571.
(14) Zhang, Z.; Greenblatt, M.; Goodenough, J. B. *J. Solid State Chem.***1994**, *108*, 402−409.
(15) Greenblatt, M. *Curr. Opin. Solid State Mater. Sci.* **1997**, *2*, 174−183.
(16) Ling, C. D.; Argyriou, D. N.; Wu, G. Q.; Neumeier, J. J. *J. Solid State Chem.* **2000**, *152*, 517−525.
(17) Ganguly, P.; Rao, C. N. R. *J. Solid State Chem.* **1984**, *53*, 193−216.
(18) Mohan Ram, R. A.; Ganaphathi, L.; Ganguly, P.; Rao, C. N. R. *J. Solid State Chem.* **1986**, *63*, 139−147.
(19) Sreedhar, K.; McElfresh, M.; Perry, D.; Kim, D.; Metcalf, P.; Honig, J. M. *J. Solid State Chem.* **1994**, *110*, 208−215.
(20) Kobayashi, Y.; Taniguchi, S.; Kasai, M.; Sato, M.; Nishioka, T.; Kontani, M. *J. Phys. Soc. Jpn.* **1996**, *65*, 3978−3982.
(21) Greenblatt, M.; Zhang, Z.; Whangbo, M. H. *Synth. Met.* **1997**, *85*, 1451−1452.
(22) Amow, G.; Davidson, I. J.; Skinner, S. J. *Solid State Ionics* **2006**, *177*, 1205−1210.

10.1021/cm070804e CCC: $37.00
Published on Web 07/17/2007

In these compounds, and because of their layered structure, the transport properties are highly anisotropic, the electronic and ionic transport maximum both being along the $a-b$ plane of the structure.[10,23−25] Therefore, for an accurate analysis of their transport properties it is necessary to use single-crystal samples or thin epitaxial films. Studies concerning the preparation of lanthanum nickel oxide epitaxial films are rather scarce, particularly for La_2NiO_4,[26−30] and have demonstrated the difficulty to prepare pure phases, intergrowth defects being common in these compounds, particularly for $n > 1$.[31] Polycrystalline La_2NiO_4 films with a different degree of orientation have been previously obtained by spray pyrolysis,[29,32] sol−gel technique,[33,34] and pulsed injection metal organic chemical vapor deposition (PIMOCVD) technique.[30,35,36] However, to our knowledge, there is only one recent report in the literature about high quality *c*-axis-oriented La_2NiO_4 epitaxial films, deposited in that case by pulsed laser deposition.[37]

In this work, we present our results on the deposition of epitaxial lanthanum−nickel oxide thin films by the liquid PIMOCVD technique. Special attention is given to the characterization of the high-temperature electronic transport properties of the epitaxial layers in order to correlate it with the observed film microstructure.

2. Experimental Section

Films have been grown by PIMOCVD using $La(thd)_3$ and $Ni(thd)_2$ (thd = tetramethylheptanedionate) as metal organic precursors dissolved in 1,2-dimethoxyethane. The molar ratio of La/Ni in the precursor solution was varied from 1 to 4 while keeping the total concentration of the solution in 0.02 M. The evaporation and deposition temperatures were fixed in 280 °C and 750 °C, respectively. The total gas flow was maintained at 1 L/h with a 1:1 ratio of oxygen and argon, and total gas pressure of 10 Torr. The opening time of the precursor injector was 2 ms with a pulse frequency of 1 Hz, and the total number of injection pulses was fixed to 1000. In each deposition run, two different types of single-crystal substrates with perovskite structure have been used to grow the films: $NdGaO_3$ (110) (noted NGO) and $SrTiO_3$ (100) (noted STO). These substrates and orientations were chosen in order to promote *c*-axis-oriented epitaxial growth of the layers because of the low mismatch with the basal perovskite plane of the $La_{n+1}Ni_nO_{3n+1}$ structure (i.e., if we consider the reported structure for $La_2NiO_{4.18}$ (LNO) in ref 14, orthorhombic with $a = 5.4652$, $b = 5.4687$, $c = 12.678$ Å cell parameters, it has a basal $a-b$ plane parameter $a_p = 3.866$ Å, which corresponds to a mismatch of +1% (tensile) on STO substrates, and from −0.08 to −0.3% (compressive) on NGO(110) substrates, depending on the crystallographic direction along the substrate plane). The phase composition and orientation of the films were analyzed by microprobe WDS analysis and X-ray diffraction (Cu Kα radiation: 1.5406 Å wavelength), respectively. We used mainly the analysis of La/Ni composition on $SrTiO_3$ (La L_α, Ni K_α, and O K_α lines) , as it provides a better accuracy than on $NdGaO_3$ because of overlapping between Nd L_l and La L_α lines of film and NGO substrate in the WDS spectra. The film thickness was determined by X-ray reflectometry for the thinner films and estimated by WDS for the thicker films. Because of the different La/Ni ratio in the solution, and in order to maintain the total La plus Ni concentration, the thickness of the films ranged from 130 to 200 nm, for film composition ratio La/Ni = 1 and 2, respectively. For the conductivity measurements, two parallel Ag contacts were painted on the surface of the samples. The planar resistance of the films was measured by AC at a fixed frequency of 1 kHz by using an HP4192A impedance analyzer, from room temperature to 670 °C in pure oxygen atmosphere. The microstructure of the layers was studied by transmission electron microscopy (TEM). Samples for TEM were prepared in cross-section; they were cut parallel to the (001) and (1-1 1) planes of the NGO substrate and mechanically ground to a thickness of about 20 μm, followed by final ion-milling under grazing incidence until electron transparency. Electron diffraction (ED) and high-resolution electron microscopy (HREM) studies were performed using a JEOL 4000EX microscope.

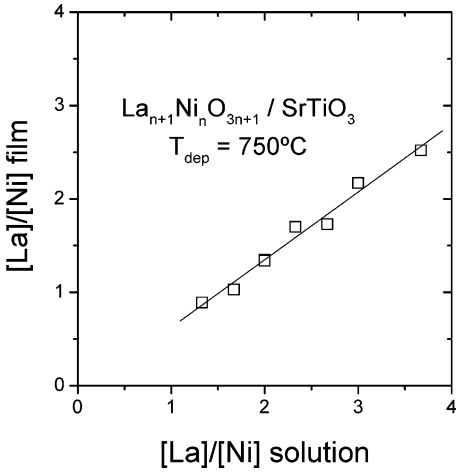

Figure 1. Correlation between measured La/Ni composition ratio in the organometallic precursor solution and in the La−Ni−O films deposited on $SrTiO_3$ substrates at 750 °C.

3. Results and Discussion

3.1. Composition and Structural Characterization of the Layers. In order to control the La/Ni ratio in the deposited film it is necessary to perform a previous calibration for each substrate temperature. Figure 1 shows the

(23) Dembinski, K.; Bassat, J. M.; Coutures, J. P.; Odier, P. *J. Mater. Sci. Lett.* **1987**, *6*, 1365−1367.
(24) Rao, C. N. R.; Buttrey, D. J.; Otsuka, N.; Ganguly, P.; Harrison, H. R.; Sandberg, C. J.; Honig, J. M. *J. Solid State Chem.* **1984**, *51*, 266−269.
(25) Minervini, L.; Grimes, R. W.; Kilner, J. A.; Sickafus, K. E. *J. Mater. Chem.* **2000**, *10*, 2349−2354.
(26) Satyalakshmi, K. M.; Mallya, R. M.; Ramanathan, K. V.; Wu, X. D.; Brainard, B.; Gautier, D. C.; Vasanthacharya, N. Y.; Hegde, M. S. *Appl. Phys. Lett.* **1993**, *62*, 1233−1235.
(27) Chen, P.; Xu, S. Y.; Zhou, W. Z.; Ong, C. K.; Cui, D. F. *J. Appl. Phys.* **1999**, *85*, 3000−3002.
(28) Dobin, A. Yu.; Nikolaev, K. R.; Krivorotov, I. N.; Wentzcovitch, R. M.; Dan Dahlberg, E.; Goldman, A. M. *Phys. Rev. B* **2003**, *68*, 113408.
(29) Raju, A. R.; Aiyer, H. N.; Rao, C. N. R. *Chem. Mater.* **1995**, *7*, 225−231.
(30) Faucheux, V.; Audier, M.; Pignard, S. *Appl. Surf. Sci.* **2006**, *252*, 5504−5507.
(31) Drennan, J.; Tavares, C. P.; Steele, B. C. H. *Mater. Res. Bull.* **1982**, *7*, 621−626.
(32) Abrutis, A.; Teiserskis, A.; Garcia, G.; Kubilius, V.; Saltyte, Z.; Salciunas, Z.; Faucheux, V.; Figueras, A.; Rushworth, S. *J. Membr. Sci.* **2004**, *240*, 113−122.
(33) Li, C.; Hu, T.; Zhang, H.; Chen, Y.; Jin, J.; Yang, N. *J. Membr. Sci.* **2003**, *226*, 1−7.
(34) Fontaine, M. -L.; Laberty-Robert, C.; Ansart, F.; Tailhades, P. *J. Solid State Chem.* **2004**, *177*, 1471−1479.
(35) Faucheux, V.; Pignard, S.; Audier, M. *J. Solid State Chem.* **2004**, *177*, 4616−4625.
(36) Faucheux, V.; Pignard, S.; Audier, M. *J. Crystal Growth* **2005**, *275*, e947−e951.
(37) Kim, G.; Wang, S.; Jacobson, A. J.; Chen, C. L. *Solid State Ionics* **2006**, *177*, 1461−1467.

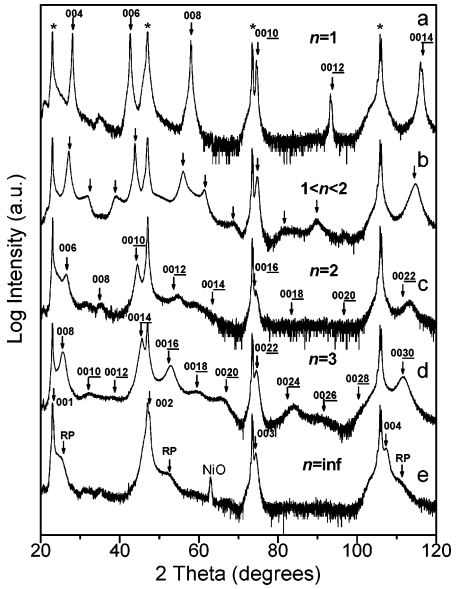

Figure 2. XRD patterns of films deposited on $NdGaO_3(110)$ substrates with different La/Ni ratio values of 2.0 (a), 1.7 (b), 1.5 (c), 1.34 (d), and 1.0 (e). The arrows indicate the expected positions for the 00*l* peaks corresponding to *c*-axis-oriented samples of the different $La_{n+1}Ni_nO_{3n+1}$ pure phases of the R-P series: La_2NiO_4 ($n = 1$), $La_3Ni_2O_7$ ($n = 2$), $La_4Ni_3O_{10}$ ($n = 3$), and $LaNiO_3$ ($n = \infty$). Substrate *hh*0 reflections are indicated with an asterisk. The reflections indicated with arrows in part b could not be indexed with any R-P phase. The film in part e shows also the presence of weak peaks, which could correspond to a RP phase with a high *n* value.

relation between the La/Ni ratio measured in films deposited at 750 °C on STO substrates as a function of the La/Ni ratio in the precursor solution. A linear correlation is clearly observed. The slope of the curve is about 0.7, making the La/Ni ratio in the film lower than in the solution for the whole composition range. This deviation in the composition transfer is typical for the MOCVD processes and is due to the different deposition efficiency for La and Ni precursors.

The XRD patterns of the films with varying La/Ni molar ratio are shown in Figure 2, for the films deposited on NGO substrates. Along with substrate reflections (indicated by * in the figure), we observed intense reflections, which match very well those of the main 00*l* reflections of different phases in the RP series. This observation confirmed the high degree of *c*-axis orientation of the layers. From the position of the X-ray diffraction peaks, the films with a La/Ni ratio close to 2 (Figure 2a), 1.5 (Figure 2c), and 1.34 (Figure 2d) were apparently composed by pure phase Ruddlesden−Popper structures La_2NiO_4 ($n = 1$), $La_3Ni_2O_7$ ($n = 2$), and $La_4Ni_3O_{10}$ ($n = 3$), respectively. For those samples, the *c*-axis parameters were measured to be 1.2715, 2.0310, and 2.7962 nm, respectively, in agreement with the corresponding RP phases. However, in the films with $n = 2$ and $n = 3$, there is a slight broadening of the diffraction peaks, along with a low relative intensity of the weaker peaks that did not reach the expected values of the pure phases. These observations could be an indication of the presence of defects in the structure.

In the films with an intermediate value of La/Ni = 1.7 (Figure 2b), between the La/Ni composition of $n = 1$ and $n = 2$ phases, the diffraction patterns did not show any evidence of the presence of extended regions of either $n = 1$ or $n = 2$ phases. Instead, the diffraction pattern shows a single set of peaks in average positions, corresponding to a combination of different RP phases (Figure 2b) as it would correspond to an intergrowth structure with domain thickness below the coherence length of the X-rays. For La/Ni close to 1 (La/Ni of about 1.6 in solution, in Figure 2d) the films present the 00*l* reflections of perovskite $LaNiO_3$ cubic structure ($n = \infty$), along with a weak peak corresponding to (110)-oriented NiO domains. The *c*-axis parameter measured for the $LaNiO_3$ structure was 0.384 nm. In this last sample, the asymmetry of the peaks, that show a broad shoulder on their higher angle side, was attributed to the presence of a RP secondary phase with a high *n* value. However, no further evidence of the presence of this phase has been observed.

The *c*-axis parameter in these compounds can vary substantially depending on the oxygen content and, in particular for thin films, it might be affected by the strain induced as a result of the substrate mismatch. This makes difficult any comparison between the films only based in cell parameters derived from a particular 00*l* reflection. Instead, we can examine the relative peak positions. Regardless the *c*-axis parameter, and in a perfectly periodical structure along the *c*-axis, the relative peak positions of two 00*l* and 00*l*′ reflections should verify: $\sin\theta_{l'}/\sin\theta_l = l'/l$, which derives simply from Bragg's law. In the case of the $La_{n+1}Ni_nO_{3n+1}$ RP series we can derive an empirical relationship between the relative angular positions and the La/Ni composition. If we take only into consideration the two main peaks 00*l* and 00*l*′ in the 2θ range between 20 and 50 degrees, they correspond to $l'/l = 6/4$ for $n = 1$; 10/6 for $n = 2$; 14/8 for $n = 3$, and 2/1 for $n = \infty$, which can be expressed as $l'/l = (2n + 1)/(n + 1)$ for the different *n* values. Since La/Ni composition ratio in $La_{n+1}Ni_nO_{3n+1}$ is $(n + 1)/n$, we can derive a general expression for the RP pure phases: $\sin\theta_{l'}/\sin\theta_{l'} = l\text{ '}/l = (2n + 1)/(n + 1) = 1 + (\mathrm{La/Ni})^{-1}$. Figure 3 shows the measured angular position ratio from the XRD pattern against the experimental La/Ni composition ratio for the set of films in our experiment, along with the expected dependence for pure RP phases with different n value (dashed curve in the figure). All the films follow very closely the expected dependence, particularly those films on NGO substrates. The films with La/Ni ratio close to 2, 1.5, 1.34, and 1.0 lay in the positions as if they corresponded to $n = 1$, $n = 2$, $n = 3$, and $n = \infty$ pure phases, respectively. The peak position ratio for the film with La/Ni = 1.7 lies along the same curve between $n = 1$ and $n = 2$. This means that all La and Ni in the films are exclusively forming RP phases, since any La or Ni excess participating of a secondary phase would cause a deviation from the above-mentioned dependence. For films with La/Ni composition ratio above 2, the peak position ratio remains equal to 1.5, as it corresponds to La_2NiO_4, and La excess forms other secondary phases, such as La_2O_3. In the same way for La/Ni composition ratio below La/Ni = 1, the films consist of $LaNiO_3$ perovskite, with peak position ratio 2.0, and Ni in excess is forming some secondary phases, such as NiO, as observed in the diffraction pattern for some films.

Similar results were obtained on STO substrates, although for some La/Ni compositions we observed a more complex intermixing of different RP phases, in comparison with films deposited on NGO under the same conditions. This was

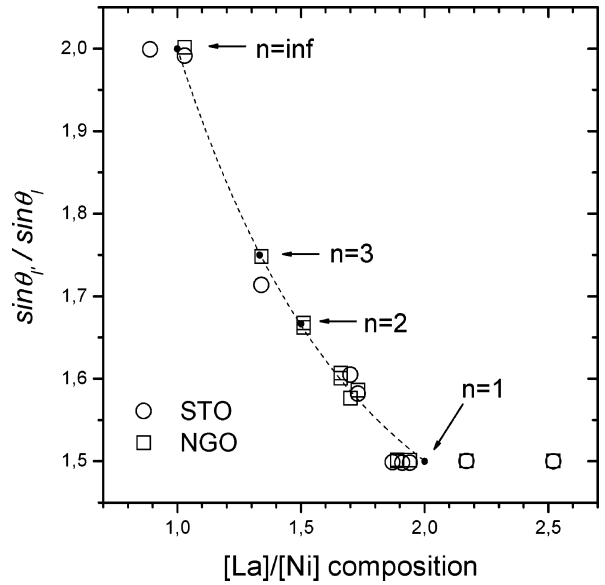

Figure 3. Dependence of the relative angular positions (expressed as sin θ) for the two main reflections 00l and 00l' in the 2θ range between 20° and 50° for the deposited films with different La/Ni composition on $NdGaO_3$ and $SrTiO_3$ substrates. The dashed curve corresponds to the expected dependence for pure Ruddlesden−Popper $La_{n+1}Ni_nO_{3n+1}$ phases, as discussed in the text. The arrows indicate the positions for pure $n = 1$, 2, 3, and ∞ phases. (The corresponding set of reflections are: $l' = 6$ and $l = 4$ for $n = 1$, 10 and 6 for $n = 2$, 14, and 8 for $n = 3$, and 2 and 1 for $n = \infty$).

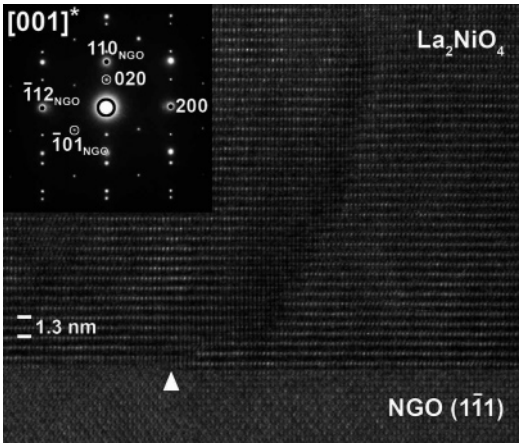

Figure 4. Cross-section HREM image and ED pattern of the film with La/Ni = 2 deposited on NGO(110) substrate, which corresponds to *c*-axis-oriented La_2NiO_4 ($n = 1$) phase. An antiphase boundary is generated in the film by the presence of a step on the substrate surface (indicated by a white arrowhead).

probably caused by the larger mismatch, of about 1%, between film and STO substrate. For a better understanding of the fundamental phenomena in this study we focused in the results on NGO substrates.

3.2. Film Microstructure. In order to assess the high quality and epitaxial growth of the films as well as to determine the real microstructure, transmission electron microscopy (TEM) was performed for the films with La/Ni = 2, 1.7, 1.5, and 1.34 on NGO substrates. Figure 4 shows a high-resolution (HREM) image of the cross-section of the film with La/ Ni = 2, along with the corresponding ED pattern. The image clearly shows the high quality of the epitaxial growth of the film with a period of about 1.3 nm, which is consistent with the *c*-parameter of La_2NiO_4 ($n = 1$) measured by XRD. The ED pattern is a superposition of

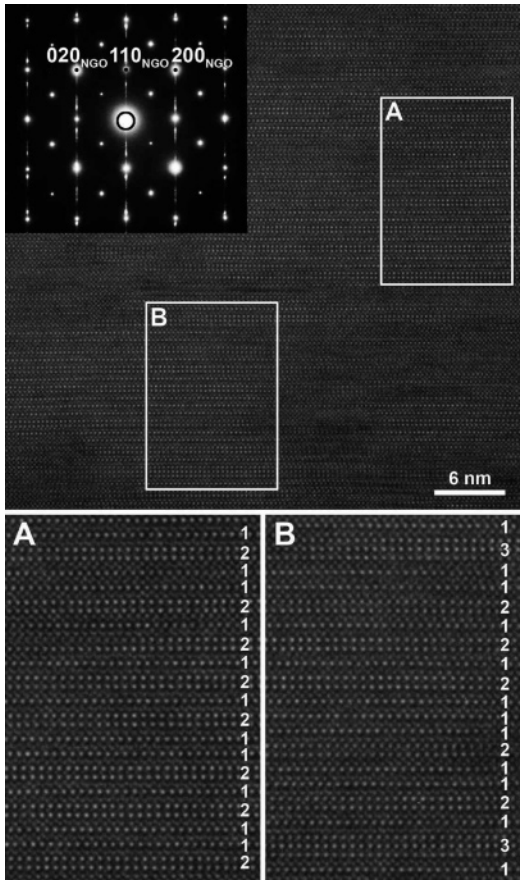

Figure 5. Cross-section HREM image and corresponding ED pattern of the film with La/Ni = 1.7 deposited on NGO. The image shows a highly defective stacking sequence of single and double perovskite-type layers. The insets are magnified images of of two different regions with (A) an apparent higher degree of a local periodic arrangement consisting of one double and single perovskite layer sequence, and (B) a lower degree of order. The average *n* value calculated from the image is 1.45.

the patterns from substrate and film and confirmed the 3D epitaxial arrangement of both structures as observed by XRD. The interface between film and substrate is sharp and well defined. However, we could observe the presence of antiphase boundary defects originated by the presence of steps on the substrate surface (indicated by an arrowhead in the image). A careful examination using HREM revealed a more complex situation in films with lower La/Ni composition values, as already suspected from the XRD patterns. Figure 5 shows the HREM cross-section image of the La/Ni = 1.7 film. A very defective intergrowth structure parallel to the substrate surface is observed, indicated by the streaking of the intensity distribution along *c** in the ED pattern from the film. A more detailed observation shows that the films consist of intermixed regions with different stacking sequences. The number of consecutive perovskite layers separated by rock salt layers is indicated in the figures. Generally, we found regions with a nonperiodical sequence of single and double perovskite layers (such as region B in Figure 5), where the bright dots represent columns of heavy atoms of two somehow different intensities: dark layers correspond to the rock-salt slabs and bright layers to the perovskite-type ones. In those regions the average La/Ni composition lays clearly between 2 and 1.5, which would correspond to La_2NiO_4 ($n = 1$, stacking sequence of single perovskite layers) and $La_3Ni_2O_7$ ($n = 2$, double perovskite

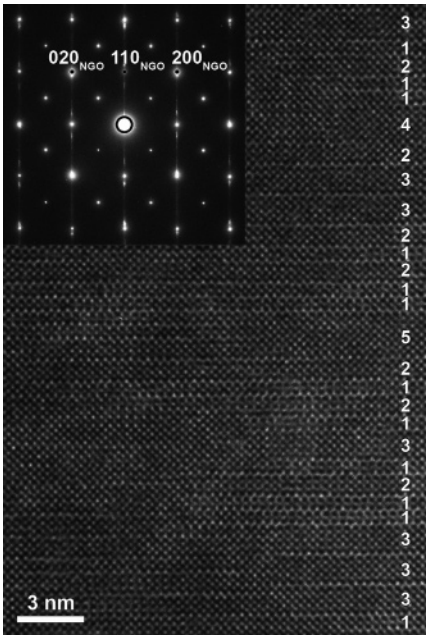

Figure 6. Cross-section HREM image and corresponding ED pattern of the film with La/Ni = 1.50 deposited on NGO. The film consists mainly of intermixed regions of $n = 1$, 2 and 3. The average n value calculated from the image is 2.0.

layers), respectively. Locally, we could observe regions with a periodic sequence of one single perovskite layer and one double perovskite layer (such as region A in Figure 5), which would correspond to La/Ni = 1.67 very close to the nominal value 1.7 of the film. The average n value calculated from the different regions in the image is about 1.45.

The cross-section of the films with La/Ni = 1.5 (in Figure 6), which seemed to correspond to $n = 2$ phase from the X-ray diffraction patterns, also shows a very defective stacking sequence composed basically by intermixed regions of $n = 1$, 2, and 3 stacks. As in the case before, the ED patterns show the streaking of the film peaks along c^* induced by the high density of planar defects. However, the average n value taken from the image remains very close to 2 as it corresponds to La/Ni = 1.5.

Similarly, the cross-section of the films with La/Ni = 1.34 (in Figure 7), also shows a very defective stacking sequence, evidenced by the streaking in the ED patterns. Despite the diffraction pattern, that suggested that this film corresponded to pure $n = 3$ phase, it is composed mainly by intermixed regions of $n = 2$, 3 and 4 domains. Small areas of higher n sequence were also observed. The average n value estimated from the image was about 3.4, slightly higher than the expected $n = 3$ for La/Ni = 1.33.

The HREM cross-section and the ED pattern of the films with La/Ni = 1.0 (shown in Figure 8) demonstrated the formation of $LaNiO_3$ perovskite with epitaxial cube-on-cube arrangement on the NGO substrate, if one considers the pseudocubic cells of $LaNiO_3$ and NGO. According to the ED pattern, that has been indexed for $LaNiO_3$ in the trigonal R-3c group, the (012)$LaNiO_3$ plane is parallel to (110)-$NdGaO_3$. The arrows in the figure indicate the presence of planar defects perpendicular to the interface, which correspond to twinned $LaNiO_3$ domains of about 3 to 10 nm thickness. No evidence of the presence of other RP phases was detected in this sample.

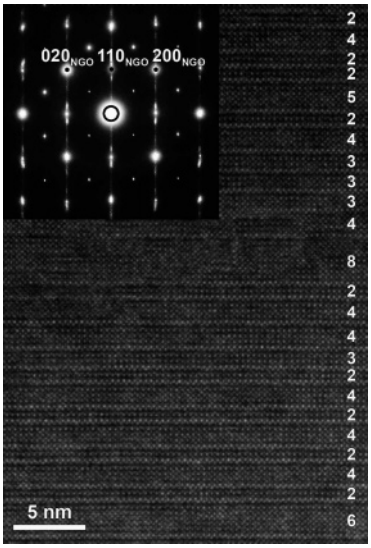

Figure 7. Cross-section HREM image and corresponding ED pattern of the film with La/Ni = 1.34 deposited on NGO. The film consists mainly of intermixed regions of $n = 2$, 3 and $n = 4$. The average n value calculated from the image is 3.4.

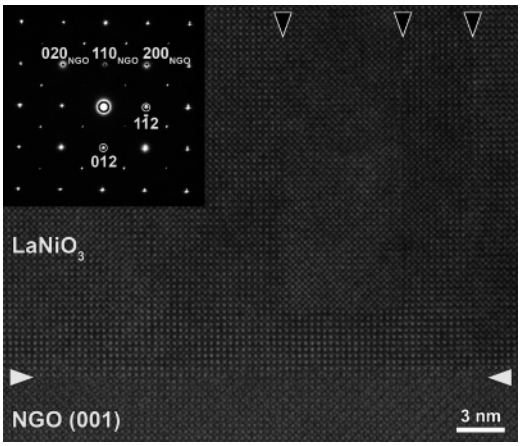

Figure 8. Cross-section HREM image and corresponding ED pattern of the film with La/Ni = 1.0 deposited on NGO. The film consists purely of perovskite $LaNiO_3$ regions. The arrows indicate vertical planar defects separating twinned domains.

In general, for the films with La/Ni composition ratio between 1 and 2, we observed intermixed phases, and the extent of the periodicity along the c-axis never exceeds the 10 nm length, so the X-ray diffraction gives peaks corresponding to average interplanar spacing with a peak broadening that reflects the very small coherence length of the crystal domains.

Our observation confirmed the difficulties to obtain pure phases of higher members ($n = 2$, 3,..) of the RP series in the La−Ni−O system, induced by the narrow domain of stability for those phases as expected from thermodynamic analysis in the La−Ni−O system, in contrast with the far more stable La_2NiO_4 phase.[38] This instability is enhanced when growing c-axis-oriented thin films from the vapor phase, because any small fluctuation of the La/Ni composition during growth will locally turn into defects in the stacking sequence, giving rise to the intergrowth of different $La_{n+1}Ni_nO_{3n+1}$ domains.

(38) Zinkevich, M.; Aldinger, F. *J. Alloys Compd.* **2004**, *375*, 147−161.

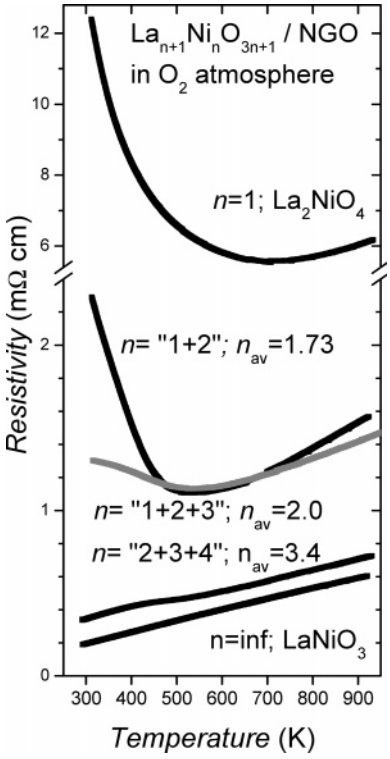

Figure 9. High temperature planar resistivity under oxygen atmosphere of the epitaxial films with different La/Ni composition deposited on NGO substrates. For each curve is indicated the corresponding film microstructure and average *n* value. The progressive change from semiconducting to metallic character is patent upon increasing *n* value between films.

3.3. High-Temperature Electronic Transport Properties. Figure 9 shows the variation of the planar resistivity in a pure O_2 atmosphere as a function of temperature of the *c*-oriented $La_{n+1}Ni_nO_{3n+1}$ films with different La/Ni composition, deposited on $NdGaO_3$ substrates. As a general trend, the resistivity of the films decreases progressively upon decreasing the average composition in the films from La/Ni = 2 to 1, and the temperature dependence reveals a change from semiconducting to metallic behavior, in the same way as expected from the results of bulk materials in the literature where the resistivity of $La_{n+1}Ni_nO_{3n+1}$ decreases with *n*, i.e., the number of perovskite layers in the structure, from semiconducting La_2NiO_4 ($n = 1$) to a normal metal $LaNiO_3$ ($n = \infty$).[18−20,22]

In more detail, the film with La/Ni = 2.0, corresponding to $La_2NiO_{4+\delta}$ ($n = 1$), showed a resistivity of about 10 mΩcm at 300 K. This value is lower than those reported for ceramic samples, but similar to the resistivity measured on single crystals along the $a-b$ plane,[23,24] which confirms the high quality of our *c*-axis-oriented La_2NiO_4 films. At temperatures below 700 K, $La_2NiO_{4+\delta}$ exhibits the expected semiconductor-type electronic conductivity, which occurs via hopping of *p*-type charge carriers between mixed-valence nickel cations.[11] The observed apparent change of the resistivity at temperatures above 700 K to a metallic-like dependence has already been found in $La_2NiO_{4+\delta}$ ceramics[9,10] and single crystal,[10,23,24] and has been attributed to a decreasing hole concentration to compensate the extensive oxygen losses from lattice upon heating.

The film with composition close to La/Ni = 1.7, which consisted of intermixed $n = 1$ and $n = 2$ phases, showed a broad semiconducting-to-metallic transition when increasing the temperature above 500 K. The room-temperature resistivity was about 2.30 mΩcm. A very similar dependence was observed for the film with an average La/Ni = 1.5 composition, which consisted mainly of intermixed $n = 1$, 2, and 3 domains. The film shows a resistivity of 1.30 mΩcm at 300 K, and it also changes from a semiconducting to a metallic dependence above 500 K. For these two films the linear temperature dependence of the resistivity above 500 K is a clear signature of the metallic state, so we have to rule out the possibility of a progressive loss of charge carriers, as it was the case for the semiconducting La_2NiO_4 phase. Although, a similar type of transition from a semiconducting to a metallic state at high temperature has already been reported as an intrinsic behavior for $La_3Ni_2O_{7-\delta}$ ($n = 2$) samples,[20,22] in our case, and in view of the intermixed microstructure ($n = 1$, 2, and 3 phases), proven by the HREM observations, we could not distinguish whether this phenomenon is directly associated to the intrinsic properties of the $n = 2$ phase, or to the combination of electrical properties of the different intermixed structures in such a close proximity.

Films with an average La/Ni = 1.34 composition, which consisted mainly of intermixed $n = 2$, 3, and 4 domains, and average *n* value of 3.4, showed a metallic behavior in the whole temperature range analyzed with a resistivity of 340 $\mu\Omega$cm at 300 K. However, the resistivity shows an anomaly around 500 K consisting of a 15% resistivity decrease upon heating. A similar anomaly was also reported in the literature for ceramic samples of pure $La_4Ni_3O_{10}$ ($n = 3$) ceramic samples.[20,22] Again, even though in our films we observe a similar behavior, we cannot rule out that it might be induced by the combination of the transport properties of intermixed regions.

The films with La/Ni = 1.0 composition, mainly composed of $LaNiO_3$ ($n = \infty$) perovskite phase, showed normal metallic behavior with the resistivity, which increases linearly with the temperature from 200 $\mu\Omega$cm at 300 K, with a slope $d\rho/dT = 0.66$ $\mu\Omega$cm K^{-1} very similar to reported values for high quality $LaNiO_3$ thin films.[26−28]

4. Conclusions

In summary we have grown high quality epitaxial lanthanum nickel oxide films in a wide range of La/Ni compositions by simply varying the La/Ni composition in the precursor solution of our PIMOCVD setup.

We have obtained films which consisted of pure La_2NiO_4 ($n = 1$) and $LaNiO_3$ ($n = \infty$) phases for the extreme La/Ni ratios, above or close to 2 and below or close to 1, respectively, and films with intermixed $La_{n+1}Ni_nO_{3n+1}$ phases for intermediate La/Ni values between 2 and 1. The intermixed phases arise from planar defects in the stacking sequence along the *c*-axis during film growth. Despite the film microstructure of the mixed phases consisting of an intricate intergrowth of domains with different *n* values, the observed average *n* value is in agreement with the measured La/Ni composition ratio. Even more remarkable is the fact

that the high-temperature electronic transport properties of the films show a progressive change from a semiconducting to a metallic character, along with the described particular anomalies, which for every average *n* value are consistent with the reported values in literature for ceramic and single-crystal samples of pure phases with the corresponding *n* values. The control over the microstructure of intermixed $La_{n+1}Ni_nO_{3n+1}$ domains opens the possibility to increase, to a certain extent, the electronic conductivity of the films. It is a subject of a further study whether for the obtained microstructures there is still an efficient path for the ionic conductivity. This would lead to mixed ionic-electronic conducting nanocomposite materials with enhanced performance for their application in electrochemical devices.

Acknowledgment. The authors would like to acknowledge financial support from the Spanish Government (MAT2002-03075 and MAT2005-02601 projects), the Spanish Fuel Cell network (CSIC-Universidad), FAME network (NoE-FP6), and SGR333 project from Generalitat de Catalunya. One of the authors (M.B.) also acknowledges the support from I3P program grant.

CM070804E